



**Search for Large Extra Dimensions  
in the Mono-Photon Final State at  $\sqrt{s} = 1.96$  TeV**

The DØ Collaboration  
URL <http://www-d0.fnal.gov>  
(Dated: March 2, 2008)

We report on a search for Large Extra Dimensions in a data sample of  $1045 \text{ pb}^{-1}$  of  $p\bar{p}$  collisions at  $\sqrt{s} = 1.96$  TeV. We investigate the Kaluza-Klein graviton production with a photon and missing energy in the final state. At 95% C.L. we set limits on the fundamental mass scale  $M_D$  of 884, 864, 836, 820, 797, 797, and 778 GeV for 2, 3, 4, 5, 6, 7, and 8 extra dimensions, respectively.

*Preliminary Results for Winter 2008 Conferences*

## I. INTRODUCTION

Arkani-Hammed, Dimopoulos, and Dvali (ADD) [1] made the first attempt to solve the intriguing hierarchy problem of the Standard Model (SM) using extra spatial dimensions. In these ADD-like theories, the SM particles are confined to a 3-dimensional (3-D) brane while gravity dilute into a newly created large extra volume. The gravitons propagate in the full “bulk” space and can decay into ordinary particles only by interacting with the 3-D brane.

The compactified extra space, assumed to be a torus, has size  $R$  which is fixed by the number of extra dimensions  $\delta$  and the fundamental Planck scale in the  $(4 + \delta)$ -dimensional space-time  $M_D$ :

$$M_{Pl}^2 = 8\pi M_D^{\delta+2} R^\delta \quad (1)$$

Here,  $M_{Pl}$  is the effective Planck scale in the 4-dimensional space-time. The hierarchy problem is overcome because the single fundamental mass scale  $M_D$  is closer to the weak scale.

Due to compactification, and similarly to a particle in a box, the gravitational fields appear as a series of quantized energy states which are referred as Kaluza-Klein (KK) modes with mass splittings  $\Delta m \sim 1/R$ . For practical purposes, and for a not too large  $\delta$ , the mass splitting is so small that the different KK modes can be integrated. Therefore, a KK graviton behaves like a massive, non-interacting, stable particle, whose direct production gives an imbalance in the final state momenta and missing mass as its collider signature. The KK graviton has a continuous distribution in mass, which corresponds to the probability of emitting gravitons with different momenta in the extra dimensions. The Feynman Rules and differential cross-section for producing a Kaluza-Klein graviton are based on the effective low-energy theory that is valid below the scale  $M_D$ , and has been studied in reference [2]. In particular, the cleanest process for direct graviton production comes from events with a photon and missing transverse energy ( $\cancel{E}_T$ ) in the final state. This production arises from the sub-process  $q\bar{q} \rightarrow \gamma G_{KK}$  (see Fig. 1).

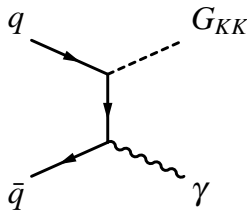


FIG. 1: Feynman diagram for the  $q\bar{q} \rightarrow \gamma G_{KK}$  process. Direct graviton production in the  $\gamma + \cancel{E}_T$  channel.

Several searches for Large Extra Dimensions (LED) have been performed by collaborations at the CERN LEP and at the Fermilab Tevatron collider [3]. In particular, the CDF experiment at Fermilab carried out a search in the mono-photon final state in Run I, setting 95% CL lower limits on the fundamental Planck scale  $M_D$  of 549, 581 and 601 GeV for 4, 6, and 8 extra dimensions, respectively.

In this note we report the results of a search for Large Extra Dimensions in the exclusive  $\gamma + \cancel{E}_T$  channel, i.e., a single photon and missing transverse energy in the final state.

## II. DATA SAMPLE

This analysis uses data recorded with the DØ detector [4] at the Fermilab Tevatron during the period between October 2002 and February 2006 using single electromagnetic (EM) object triggers which are almost 100% efficient to select signal events. It corresponds to an integrated luminosity of  $1045 \pm 63 \text{ pb}^{-1}$ .

The subsystems of the DØ detector most relevant to this analysis are the central preshower (CPS) detector and the liquid argon/uranium calorimeter. The CPS system is located in front of the calorimeter and consists of several extruded triangular layers of scintillator strips, providing precise measurement of positions of EM showers. The calorimeter has a central section (CC) covering  $|\eta|$  up to  $\approx 1.1$ , where  $\eta$  is the pseudorapidity measured with respect to the geometrical center of the detector, and two end calorimeters (EC) that extend coverage to  $|\eta| \approx 4.2$ , each of them located in separate cryostats [5]. The electromagnetic part of the calorimeter has four longitudinal layers and transverse segmentation of  $0.1 \times 0.1$  in  $\eta - \phi$  space (where  $\phi$  is the azimuthal angle), with the only exception of the third layer, where it is  $0.05 \times 0.05$ . Additionally, scintillators between the CC and EC cryostats provide sampling of developing showers at  $1.1 < |\eta| < 1.4$ .

The present study also makes use of the central-tracking and muon systems. The central-tracking system comprises a silicon microstrip tracker (SMT) and a central fiber tracker (CFT), both housed within a 2 T superconducting

solenoidal magnet, with designs optimized for tracking and vertexing at pseudorapidities  $|\eta| < 3$  and  $|\eta| < 2.5$ , respectively. The outer muon system, at  $|\eta| < 2$ , consists of a layer of tracking detectors and scintillation trigger counters in front of 1.8 T toroids, followed by two similar layers after the toroids.

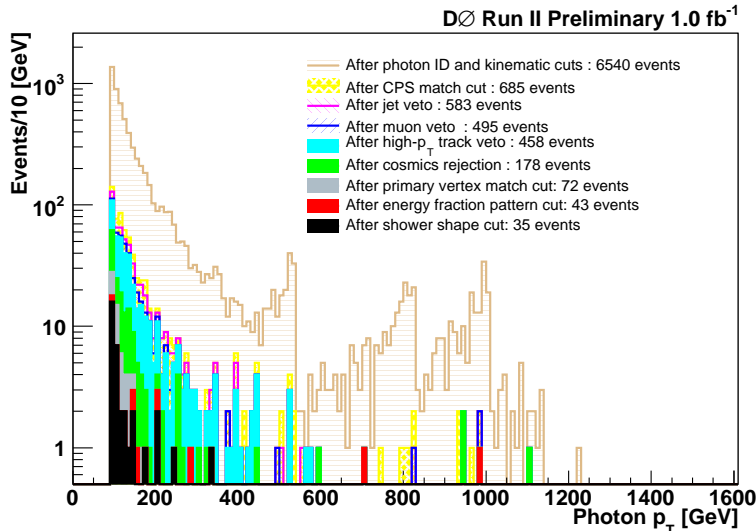


FIG. 2: Transverse momentum distribution of the photon after each selection cut.

### III. EVENT SELECTION

Photons are reconstructed as EM calorimeter clusters fulfilling all the following requirements:

- At least 90% of the energy is deposited in the EM section of the calorimeter.
- The calorimeter isolation variable  $\mathcal{I} = (E_{tot}(0.4) - E_{em}(0.2))/E_{em}(0.2)$  is less than 0.07, where  $E_{tot}(0.4)$  and  $E_{em}(0.2)$  denote the energy deposited in the calorimeter using the simple cone method of radius  $\mathcal{R} = \sqrt{(\Delta\eta)^2 + (\Delta\phi)^2} = 0.4$  and 0.2 respectively.
- Has track isolation, i.e, the scalar sum of the transverse momenta ( $p_T$ ) of all tracks which originate from the primary vertex in an annulus of  $0.05 < \mathcal{R} < 0.4$  around the cluster is less than 2 GeV.
- It is in the CC with  $|\eta| < 1.1$
- Has no associated track in the central tracking system nor a significant density of hits in the SMT and CFT systems consistent with a track.
- It is matched to a CPS cluster.

A photon sample is obtained by requiring only one photon with high transverse momentum. In particular, we require it to have minimum  $p_T$  of 90 GeV.

Additionally, no jets with  $p_T > 15$  GeV are allowed in the event. Jets are reconstructed using the iterative midpoint cone algorithm [6] with a cone size of  $\mathcal{R} = 0.5$ . The missing transverse energy – which is computed from calorimeter cells with  $|\eta| < 4$  and is corrected for the EM and jet energy scales – is required to be at least 70 GeV. This high  $\cancel{E}_T$  requirement guarantees negligible multijets background in the final candidate events without introducing large inefficiency in the signal selection.

We veto on muons and muons that are tagged as cosmic. Furthermore, in order to reject events with leptons that leave a distinguishable signature in the tracker but that are not reconstructed in the rest of the subsystems of the detector, we impose a requirement on the transverse momentum of any isolated track not to be greater than 6.5 GeV. A track is considered to be isolated if the ratio between the scalar sum of the  $p_T$  of all tracks which originate from

the primary vertex in an annulus of  $0.1 < \mathcal{R} < 0.4$  around the track and the  $p_T$  of the track is less than 0.3. This isolated high  $p_T$  track cut was optimized against minimum  $p_T$  of the track and the isolation of the track.

Additionally, we require at least one primary vertex in the event that agrees with that of the photon candidate within 10 cm. This is accomplished by the EM “pointing” algorithm which determines the angle and point of origin of the electromagnetic shower – with a resolution of about 2 cm –, independent of the determination of the primary vertex, and based only on the calorimeter and preshower cluster information.

To further reduce cosmic ray muons, we reject events that have activity in the muon and the calorimeter systems that is in agreement with a cosmic muon undergoing bremsstrahlung, i.e., events with a photon EM cluster aligning collinearly with two muon segments. In addition, we remove events with abnormal high energies due to hardware problems by applying a cut on the photon shower shape, and require that the pattern of the energy fractions deposited in the different EM layers of the calorimeter are consistent with that of an object originated from the interactions region of the detector and not from halo or cosmic particles. The last two requirements are fully efficient at accepting signal events.

The cumulative effect of this set of cuts is shown in Fig. 2. After all the selection requirements, only 35 events are selected in data.

## IV. DATA ANALYSIS

### A. Estimation of the number of events with genuine photons

Despite all the cuts aiming at removing unwanted events containing cosmics and halo particles, some contamination is still present in the final candidate events. In order to appraise this background, determine the number of misidentified jets (which mimic photons), and estimate the number of genuine photons in the selected sample, we exploit the EM pointing information of the distance of closest approach (DCA) in the  $r - \phi$  space, where  $r$  denotes the perpendicular distance from the axis along the beam direction. Misidentified jets have poor pointing resolution and therefore a wider DCA distribution (compared to photons or electrons) is expected. Likewise, one can anticipate the DCA distribution for halo and cosmic events to have an even wider DCA shape.

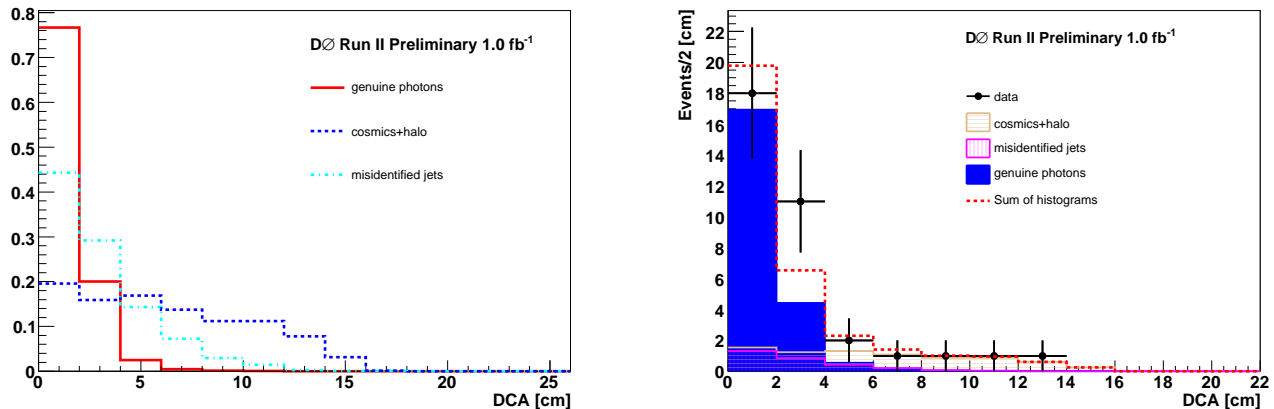


FIG. 3: Different shapes in DCA contributing to the photon sample (left). Template fit in DCA of the remaining events in data (right).

We prepare three DCA distribution templates: the cosmics+halo template, the misidentified jets template and the signal template. The first one is selected by applying the same kinematical cuts as for the photon sample, but requiring events with at least one cosmic muon plus events with no primary vertex, or with a very low track multiplicity (less than three). The misidentified jets template is obtained from the data sample with EM objects satisfying photon identification criteria but with an inverted track isolation requirement. We cross-check the shape of this distribution with the one obtained from a real data  $\gamma + jets$  sample, finding good agreement between them. The  $\gamma + jets$  sample is obtained from a large two high- $p_T$  EM objects sample. We select the photon and the jet out of the two high  $p_T$  EM objects, keeping the selection for them totally disjoint from each other. The  $\gamma$  particle fulfills all the photon selection criteria, while the other EM object is assured to be a jet by reversing all the calorimeter cuts and the track isolation. Finally, the signal template is obtained from a real data sample of isolated electrons. A small

systematic error due to the uncertainty in this DCA shape has been accounted for in the final result. The different DCA shapes can be seen in Fig. 3.

We fit the DCA distribution of the photon sample to these three contributions, taking the normalization for the misidentified-jets component from the rate of this type of objects in the real data  $\gamma + jet$  sample. The result of the fit is illustrated in Fig. 3. Most of the genuine photons are within 4 cm in DCA, therefore we limit our analysis to this particular window.

## B. SM Background Estimation

The main instrumental background comes from  $W \rightarrow e\bar{\nu}$  decays, where the electron, due to tracking inefficiency, is misidentified as a photon. This contribution to the background is estimated from data using a sample of isolated electrons. We apply the same exact cuts as for our photon sample, and multiply the remaining number of events, before the isolated high  $p_T$  track veto, by  $(1 - \epsilon_{trk})/\epsilon_{trk}$ , where  $\epsilon_{trk}$  is the track match efficiency estimated to be  $0.985 \pm 0.001$  [7]. We then multiply this number by the efficiency of each of the remaining cuts: high  $p_T$  track cut, cosmic events rejection, primary vertex match requirement, and the DCA 4 cm window requirement. These efficiencies are measured in data using  $W \rightarrow e\nu$  events and are determined to be  $0.0865 \pm 0.004$ ,  $0.909 \pm 0.004$ ,  $0.942 \pm 0.003$  and  $0.968 \pm 0.003$  respectively.

Smaller instrumental contributions to the background are expected from  $W + \gamma$  production where the charged lepton in a leptonic  $W$  decay is lost, and from jets misidentified as photons. The  $W + \gamma$  background is estimated using Monte Carlo  $W(+jets) \rightarrow lepton + \bar{\nu}(+jets)$  samples (generated with PYTHIA [8]). We extract  $W + \gamma$  events at generator level, separating the final state radiation component from the resulting sub-sample in order to weight the events by the cross-sections calculated with the Baur MC generator [9], which properly handles the contributions to the full process. The leading order cross-section is multiplied by a k-factor of 1.335 to compensate for NLO multijets effects. The results for the production cross-sections are: 8.76 pb and 1.85 pb, for final state radiation and interference components respectively. The CTEQ6L parton distribution functions (PDF) were used in this calculation. Additionally, we are careful not to include misidentified jets in the estimation by requiring the generated photon to match the reconstructed one.

The only physics background to the  $\gamma + \cancel{E}_T$  final state comes from the process  $q\bar{q} \rightarrow Z\gamma \rightarrow \nu\bar{\nu}\gamma$ . This irreducible contribution is estimated from Monte Carlo using a sample generated with PYTHIA program version 6.3. The production cross section for central photons with  $p_T > 90$  GeV – when jets with a transverse energy larger than 15 GeV are excluded – corresponds effectively to the one at LO: 29.06 fb. When calculating the expected number of events from this process, we account for the small  $p_T$ -dependent difference at NLO that the k-factor introduces for this range of photon transverse momentum [10].

Monte Carlo events for both,  $W + \gamma$  and  $Z + \gamma$ , were passed through a detector simulation based on GEANT [11] package, and reconstructed using the same reconstruction software as for the data. Additionally, we apply a scale factor which accounts for the differences between the efficiency determinations from data and simulation.

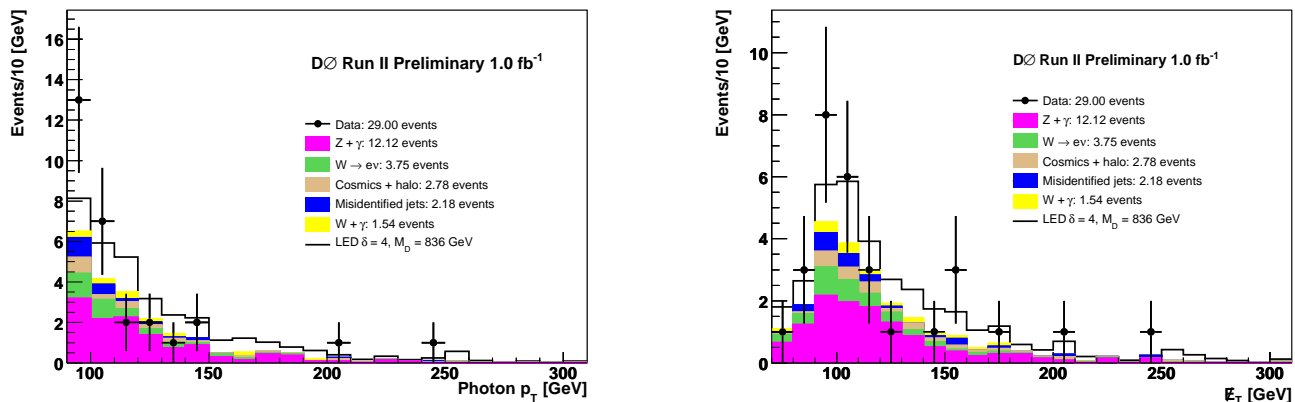


FIG. 4: Photon  $p_T$  distribution (left) and  $\cancel{E}_T$  distribution (right) for the final event candidates, after all the applied cuts. SM backgrounds are stacked on top of each other.

Table I shows a summary of the different types of background that were estimated using data and MC. These results include the uncertainty on the SM cross-sections – which is dominated by the uncertainty on the k-factor

TABLE I: Background contribution estimated using data and MC.

Background	Number of expected events
Cosmic + halo	$2.78 \pm 1.41$
Misidentified jets	$2.18 \pm 1.52$
$W \rightarrow e\bar{\nu}$	$3.75 \pm 0.26$
$Z + \gamma \rightarrow \nu\bar{\nu}\gamma$	$12.12 \pm 1.30$
$W + \gamma$	$1.54 \pm 0.21$
Total Background	$22.37 \pm 2.50$
Data	29

(7%)–, uncertainty in the photon identification efficiency (5%), and the uncertainty in the total integrated luminosity (6.1%).

We discard possible  $\gamma+jet$  background (where the jet is not reconstructed), or any other extra source of background, by releasing the  $\cancel{E}_T$  requirement in the analysis and performing an exponential fit to the difference between the photon sample data and the total accounted background at low values of  $\cancel{E}_T$ . The multijets contribution becomes negligible at values of missing transverse energy higher than 70 GeV.

Fig. 4 shows the photon  $p_T$  distribution, with all the SM backgrounds stacked on top of each other, as well as the missing transverse energy for the final event candidates after all the applied cuts.

## V. SIGNAL MONTE CARLO AND LIMITS SETTING

We generate the signal MC with  $M_D = 1.5$  TeV for number of extra dimensions  $\delta = 2, 3, 4, 5, 6, 7$  and 8. The PYTHIA program is used to generate around 1000 events for each number of extra dimensions. For different values of  $M_D$ , the cross-section scales as  $1/M_D^{\delta+2}$ , leaving the kinematical spectra unaffected for a fixed number of extra dimensions. The signal efficiencies are independent of  $M_D$ . Fig. 5 (left) shows the signal cross-section curves for the different values of  $\delta$ , for photons with  $p_T > 90$  GeV that are within  $|\eta| < 1.1$ .

Similarly to the SM Monte Carlo backgrounds, the generated signal events were passed through the GEANT-based detector simulation and later reconstructed with the DØ reconstruction software. The photon identification efficiency contributes 5% uncertainty to the signal acceptance. Additionally, we assign PDFs uncertainty of 4%, and 6.1% due to the measurement of integrated luminosity.

As seen in table I, data and SM expectation agree, and we do not see any significant excess of events, so we proceed to set lower limits for the fundamental Planck scale  $M_D$ . We use a likelihood fitter [12] to set limits on the production cross section. This fitter incorporates a log-likelihood ratio (LLR) test statistic method and utilizes binned  $p_T$  distributions rather than a single-bin (fully-integrated) value. This allows to account for the shapes of the distributions and gain greater sensitivity. Table II and Fig. 5 (right) summarize the limit setting results.

TABLE II: Summary of limits calculation.

$\delta$	Total Efficiency	Excluded cross-section fb	$M_D$ lower limit GeV	Expected cross-section fb	$M_D$ lower expected limit GeV
2	$0.4905 \pm 0.0442$	27.61	884	23.39	921
3	$0.4834 \pm 0.0435$	24.49	864	22.73	877
4	$0.4715 \pm 0.0425$	24.96	836	22.83	848
5	$0.4285 \pm 0.0387$	25.03	820	24.77	821
6	$0.4979 \pm 0.0450$	25.35	797	22.29	810
7	$0.4921 \pm 0.0444$	23.98	797	23.06	801
8	$0.5215 \pm 0.0471$	24.20	778	21.89	786

## VI. ACKNOWLEDGMENTS

We thank Stephen Mrenna and Steve Muanza for their invaluable help, the staffs at Fermilab and collaborating institutions, and acknowledge support from the DOE and NSF (USA); CEA and CNRS/IN2P3 (France); FASI, Rosatom and RFBR (Russia); CAPES, CNPq, FAPERJ, FAPESP and FUNDUNESP (Brazil); DAE and DST (India); Colciencias (Colombia); CONACyT (Mexico); KRF and KOSEF (Korea); CONICET and UBACyT (Argentina);

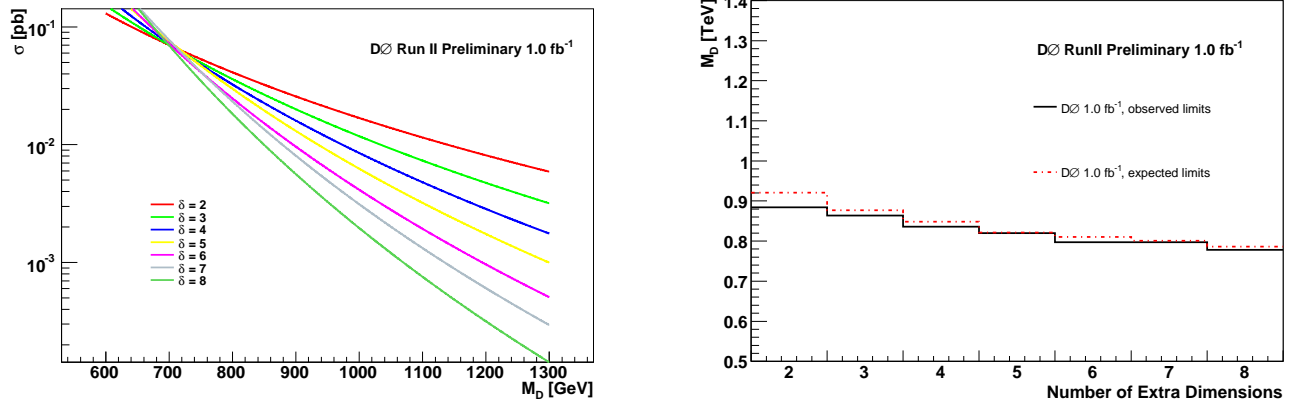


FIG. 5: Signal cross section curves for the different values of  $\delta$ , for photons with  $p_T > 90$  GeV that are within  $|\eta| < 1.1$  (left). Observed and expected lower limits on  $M_D$  for LED in the  $\gamma + \cancel{E}_T$  final state (right).

FOM (The Netherlands); STFC (United Kingdom); MSMT and GACR (Czech Republic); CRC Program, CFI, NSERC and WestGrid Project (Canada); BMBF and DFG (Germany); SFI (Ireland); The Swedish Research Council (Sweden); CAS and CNSF (China); and the Alexander von Humboldt Foundation.

- 
- [1] N. Arkani-Hamed, S. Dimopoulos, G. Dvali, Phys. Lett. B **429**, 263 (1998).  
[2] G. Guidice, R. Rattazzi, and J. Wells, Nucl. Phys. B **544**, 3 (1999).  
[3] G. Landsberg, “Collider Searches for Extra Dimensions”, arXiv:hep-ex/0412028 v2, and references therein.  
[4] V.M. Abazov *et al.* (DØ Collaboration), Nucl. Instrum. Methods A **565**, 463 (2006).  
[5] S. Abachi *et al.* (DØ Collaboration), Nucl. Instrum. Methods Phys. Res. A **338**, 185 (1994).  
[6] G. C. Blazey *et al.*, in *Proceedings of the Workshop: QCD and Weak Boson Physics in Run II* edited by U. Baur, R.K. Ellis, D. Zeppenfeld, FERMILAB-PUB-00/297 (2000).  
[7] V.M. Abazov *et al.*, Phys. Lett. B **659**, 856 (2008).  
[8] T. Sjöstrand *et al.*, Comput. Phys. Commun. **135**, 238 (2001).  
[9] U. Baur and E. Berger, Phys. Rev. D **41**, 1476 (1990).  
[10] U. Baur, T. Han, “QCD Corrections and Anomalous Couplings in  $Z\gamma$  Production at Hadron Colliders”, arXiv:hep-ph/9710416.  
[11] R. Brun and F. Carminati, CERN Program Library Long Writeup W5013, 1994.  
[12] W. Fisher, FERMILAB-TM-2386-E (2007); T. Junk, Nucl. Instrum. Methods A **434**, 435 (1999); A. Read, “Modified Frequentist Analysis of Search Results (The CLs Method)”, CERN 2000-005 (2000).